

# Mononuclear Nonheme High-Spin ( $S=2$ ) versus Intermediate-Spin ( $S=1$ ) Iron(IV)–Oxo Complexes in Oxidation Reactions

Seong Hee Bae<sup>†</sup>, Mi Sook Seo<sup>†</sup>, Yong-Min Lee, Kyung-Bin Cho, Won-Suk Kim, and Wonwoo Nam<sup>\*</sup>

**Abstract:** Mononuclear nonheme high-spin ( $S=2$ ) iron(IV)–oxo species have been identified as the key intermediates responsible for the C–H bond activation of organic substrates in nonheme iron enzymatic reactions. Herein we report that the C–H bond activation of hydrocarbons by a synthetic mononuclear nonheme high-spin ( $S=2$ ) iron(IV)–oxo complex occurs through an oxygen non-rebound mechanism, as previously demonstrated in the C–H bond activation by nonheme intermediate ( $S=1$ ) iron(IV)–oxo complexes. We also report that C–H bond activation is preferred over C=C epoxidation in the oxidation of cyclohexene by the nonheme high-spin (HS) and intermediate-spin (IS) iron(IV)–oxo complexes, whereas the C=C double bond epoxidation becomes a preferred pathway in the oxidation of deuterated cyclohexene by the nonheme HS and IS iron(IV)–oxo complexes. In the epoxidation of styrene derivatives, the HS and IS iron(IV) oxo complexes are found to have similar electrophilic characters.

Mononuclear nonheme iron enzymes activate dioxygen ( $O_2$ ) to carry out metabolically important oxidative transformations by generating high-spin ( $S=2$ ) iron(IV)–oxo intermediates that have been trapped, characterized, and shown to be competent oxidants in enzymatic reactions.<sup>[1]</sup> In 2003, the first nonheme iron(IV)–oxo intermediate was characterized spectroscopically in the reaction of taurine dioxygenase (TauD) and the first X-ray crystal structure of a synthetic nonheme iron(IV)–oxo complex, [(TMC)Fe<sup>IV</sup>(O)]<sup>2+</sup> (TMC = 1,4,8,11-tetramethyl-1,4,8,11-tetraazacyclotetradecane), was reported as a model compound of nonheme iron enzyme intermediates.<sup>[2]</sup> Since then, a large number of mononuclear nonheme iron(IV)–oxo complexes have been synthesized and investigated intensively to elucidate their structural and spectroscopic properties as well as to study the reactivities of the novel iron(IV)–oxo intermediates in enzymatic reactions.<sup>[3]</sup> However, more than 90% of the synthetic nonheme iron(IV)–oxo complexes reported so far possess an intermediate ( $S=1$ ) ground spin state, whereas only a small number of nonheme high-spin ( $S=2$ ) iron(IV)–oxo complexes have been prepared.<sup>[4,5]</sup> Moreover, most of the

reactivity and mechanistic studies were conducted using the intermediate-spin (IS) iron(IV)–oxo complexes in nonheme iron models. In contrast, the reactivities of the high-spin (HS) iron(IV)–oxo complexes in oxidation reactions are poorly understood. In addition, although it has been proposed in density functional theory (DFT) calculations that the HS Fe<sup>IV</sup>O complexes are more reactive than the corresponding IS Fe<sup>IV</sup>O complexes in C–H bond activation reactions (that is, exchange-enhanced reactivity),<sup>[6]</sup> the reactivity differences between the mononuclear nonheme IS and HS Fe<sup>IV</sup>O complexes have yet to be demonstrated clearly in experiments. Furthermore, the reaction mechanisms and reactivity patterns of the IS and HS Fe<sup>IV</sup>O complexes in oxidation reactions have been rarely compared.<sup>[7]</sup> Thus, to understand why mononuclear nonheme iron enzymes utilize HS Fe<sup>IV</sup>O intermediates in their enzymatic reactions, a mechanistic comparison of the nonheme IS and HS Fe<sup>IV</sup>O complexes in oxidation reactions is necessary, considering especially the C–H bond activation reactions which are the primary oxidation reactions executed by nonheme iron enzymes.

In 2011, we reported a highly reactive nonheme iron(IV)–oxo complex with a ground  $S=1$  spin state [(Me<sub>3</sub>NTB)Fe<sup>IV</sup>(O)]<sup>2+</sup> (**1**; Me<sub>3</sub>NTB = tris((1-methyl-1*H*-benzo[*d*]imidazol-2-yl)methyl)amine; see Figure 1 A, C).<sup>[8]</sup> This iron(IV)–oxo complex is the most powerful oxidant among the intermediate-spin ( $S=1$ ) iron(IV)–oxo complexes reported so far.<sup>[8]</sup> More recently, Bominaar, Münck, Que, and co-workers reported the synthesis of a highly reactive high-spin ( $S=2$ ) iron(IV)–oxo complex by substituting the 1-methyl-1*H*-benzo[*d*]imidazol-2-yl moiety in the Me<sub>3</sub>NTB ligand with a quinolin-2-yl group, forming [(TQA)Fe<sup>IV</sup>(O)]<sup>2+</sup> (**2**; TQA = tris(quinolin-2-ylmethyl)amine; see Figure 1 B, D).<sup>[5]</sup> This high-spin ( $S=2$ ) iron(IV)–oxo complex is the most reactive nonheme iron(IV)–oxo oxidant reported to date in nonheme IS and HS iron(IV)–oxo complexes.<sup>[5]</sup> We therefore used these nonheme IS and HS Fe<sup>IV</sup>O complexes in reactivity studies to compare their reaction mechanisms and reactivity patterns in the C–H bond activation of alkanes (oxygen rebound versus oxygen non-rebound), the oxidation of cyclohexene (C–H bond activation versus C=C double bond epoxidation), and the epoxidation of olefins.<sup>[9–12]</sup> We now report that the reaction mechanisms and reactivity patterns of the nonheme IS and HS Fe<sup>IV</sup>O complexes are virtually the same in those reactions. Mechanistic details for the alkane hydroxylation, cyclohexene oxidation, and olefin epoxidation reactions by the IS Fe<sup>IV</sup>O complex [(Me<sub>3</sub>NTB)Fe<sup>IV</sup>(O)]<sup>2+</sup> (**1**) and the HS Fe<sup>IV</sup>O complex [(TQA)Fe<sup>IV</sup>(O)]<sup>2+</sup> (**2**) are discussed in the present study.

[\*] S. H. Bae,<sup>[†]</sup> Dr. M. S. Seo,<sup>[†]</sup> Dr. Y.-M. Lee, Dr. K.-B. Cho, Prof. Dr. W.-S. Kim, Prof. Dr. W. Nam  
Department of Chemistry and Nano Science  
Ewha Womans University  
Seoul 03760 (Korea)  
E-mail: wwnam@ewha.ac.kr

[†] These authors contributed equally to this work.

Supporting information for this article can be found under:  
<http://dx.doi.org/10.1002/anie.201603978>.

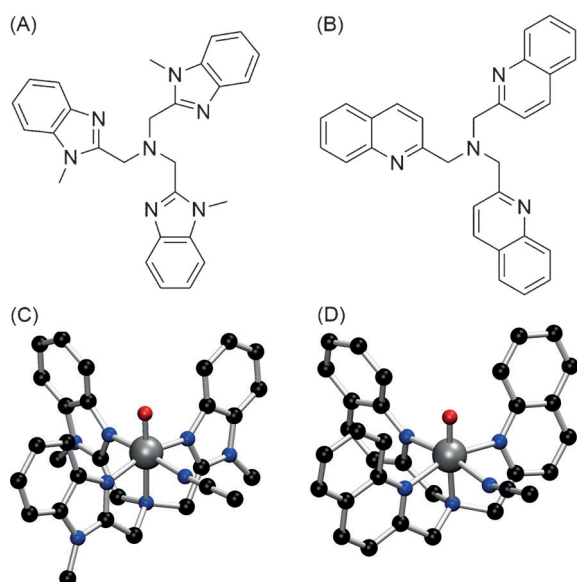
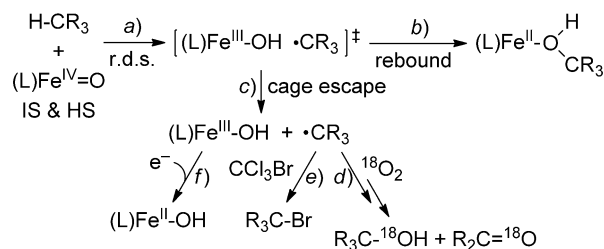


**Figure 1.** Structures of Me<sub>3</sub>NTB (A) and TQA (B) ligands and DFT-optimized structures of [(Me<sub>3</sub>NTB)Fe<sup>IV</sup>(O)]<sup>2+</sup> (C) and [(TQA)Fe<sup>IV</sup>(O)]<sup>2+</sup> (D). The coordinates for [(Me<sub>3</sub>NTB)Fe<sup>IV</sup>(O)]<sup>2+</sup> and [(TQA)Fe<sup>IV</sup>(O)]<sup>2+</sup> were taken from References [8] and [5], respectively. Atom colors: Fe = gray, O = red, N = blue, C = black.

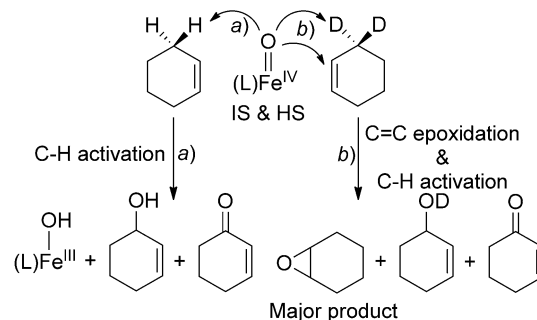
We first considered the C–H bond activation of alkanes in terms of the oxygen rebound versus oxygen non-rebound mechanisms. It has been shown that the C–H bond activation of alkanes by nonheme IS Fe<sup>IV</sup>O and other nonheme metal(IV)–oxo (M = Cr, Mn, and Ru) complexes occurs by means of an oxygen non-rebound mechanism,<sup>[9,10]</sup> not through an oxygen rebound mechanism as shown in heme iron–oxo intermediates.<sup>[13]</sup> We therefore compared the C–H bond activation mechanism(s) of nonheme IS and HS Fe<sup>IV</sup>O complexes by carrying out the hydroxylation of cyclohexane by **1** and **2** under various reaction conditions, such as under an Ar atmosphere, under an <sup>18</sup>O-labeled dioxygen (<sup>18</sup>O<sub>2</sub>) atmosphere, and in the presence of an alkyl radical scavenger (CCl<sub>3</sub>Br; Scheme 1A).

The nonheme iron(IV)–oxo complexes **1** and **2** were prepared using the reported procedures.<sup>[5,8]</sup> Upon addition of cyclohexane to the solutions of **1** and **2** at –40 °C, intermediates **1** and **2** disappeared with the first-order kinetic profile (see Figure S1 in the Supporting Information). The product analysis of the reaction solutions revealed the formation of cyclohexanol (24 ± 3%), cyclohexanone (3 ± 2%), and cyclohexene (15 ± 2%) in the reaction of **1**, whereas in the reaction of **2**, cyclohexanol (27 ± 4%), cyclohexanone (5 ± 3%), and cyclohexene (17 ± 3%) were formed (Table S1). It is of interest to note that in addition to the hydroxylated products, a significant amount of a desaturated product (that is, cyclohexene) was formed in these reactions (it has been reported that heme and nonheme iron–oxo intermediates produce desaturated products in the hydroxylation of alkanes).<sup>[9,14]</sup> Interestingly, when the hydroxylation of cyclohexane by **1** and **2** was carried out in the presence of <sup>18</sup>O<sub>2</sub> (Scheme 1A; pathway d), the product distribution was changed. Specifically, cyclohexanone was obtained as

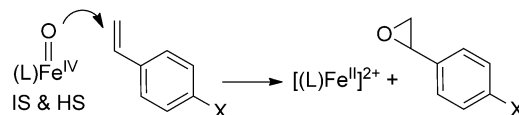
#### A. Oxygen rebound versus oxygen non-rebound mechanisms



#### B. C–H bond activation versus C=C double bond epoxidation



#### C. Comparison of electrophilic character in olefin epoxidation



**Scheme 1.** Proposed mechanisms for A) the C–H bond activation of alkanes, B) the oxidation of cyclohexene and [D<sub>10</sub>]cyclohexene, and C) the epoxidation of *para*-X-substituted styrenes by nonheme IS and HS Fe<sup>IV</sup>O complexes **1** and **2**.

a major product (see Table S1) and the oxygens in the cyclohexanol and cyclohexanone products were found to be derived from <sup>18</sup>O<sub>2</sub> (Figure S2). In addition, when we carried out the hydroxylation of cyclohexane by **1** and **2** in the presence of CCl<sub>3</sub>Br under an Ar atmosphere, we detected the formation of bromocyclohexane (about 55% yield) as the sole product (Scheme 1A; pathway e). Based on the results of the <sup>18</sup>O<sub>2</sub> and CCl<sub>3</sub>Br experiments, we conclude that after the Fe<sup>IV</sup>O intermediates abstracted a H atom from cyclohexane (Scheme 1A; pathway a), a cyclohexanyl radical escaped from the cage (pathway c) and then was trapped either by <sup>18</sup>O<sub>2</sub> (pathway d) or by CCl<sub>3</sub>Br (pathway e).

We also analyzed the decayed iron products of **1** and **2** with electron paramagnetic resonance (EPR) spectroscopy and cold-spray ionization mass spectrometry (CSI-MS). EPR spectra of the reaction solutions exhibited signals at *g* = 7.3, 4.3, and 2.00 for **1** and *g* = 7.2, 4.3, and 2.00 for **2** (Figure S3), characteristic of high-spin Fe<sup>III</sup> species (*S* = 5/2), demonstrating that iron(III) species were formed as the major products in the hydroxylation of cyclohexane by **1** and **2**. Furthermore, upon addition of decamethylferrocene (Me<sub>10</sub>Fc) to the resulting solutions (Scheme 1A; pathway f), the EPR spectra became silent (see insets in Figure S3), indicating that the Fe<sup>III</sup> species were reduced to Fe<sup>II</sup> species by the one-electron reductant. In the CSI-MS experiments, we detected ion peaks at mass-to-charge ratios *m/z* = 671.1 and 261.1 in the reaction

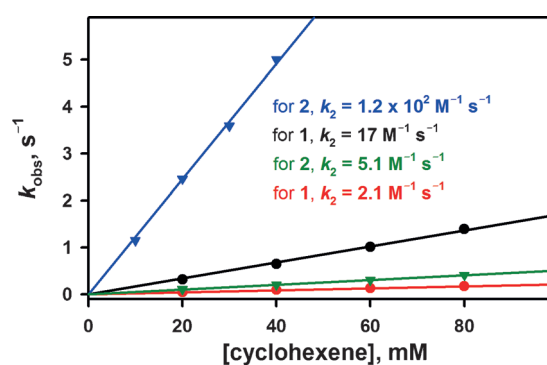
of **1** and cyclohexane (Figure S4a). These ion peaks correspond to  $[\text{Fe}^{\text{III}}(\text{OH})(\text{Me}_3\text{NTB})(\text{CF}_3\text{SO}_3)]^+$  (calculated  $m/z = 671.1$ ) and  $[\text{Fe}^{\text{III}}(\text{OH})(\text{Me}_3\text{NTB})]^{2+}$  (calculated  $m/z = 261.1$ ), respectively. In the reaction of **2** and cyclohexane, we detected one ion peak at  $m/z = 662.1$  (Figure S4b), which corresponds to  $[\text{Fe}^{\text{III}}(\text{OH})(\text{TQA})(\text{CF}_3\text{SO}_3)]^+$  (calculated  $m/z = 662.1$ ). Based on the spectroscopic analyses of iron products using EPR and CSI-MS, we conclude that  $\text{Fe}^{\text{III}}$  species, not  $\text{Fe}^{\text{II}}$  species, were formed as the decayed products of **1** and **2** (Scheme 1 A, pathways *a, c*).

For the C–H bond activation of alkanes, the experimental evidence supports an oxygen non-rebound mechanism by nonheme IS and HS  $\text{Fe}^{\text{IV}}\text{O}$  complexes (Scheme 1 A, pathways *a* and *c*) rather than the oxygen rebound mechanism (Scheme 1 A, pathways *a* and *b*), corresponding to previous work by us and others on the hydroxylation of alkanes by nonheme metal(IV)–oxo and metal(V)–oxo complexes.<sup>[7a,9,10,12,15]</sup>

We next considered chemoselectivity in the oxidation of cyclohexene, focusing on whether the reaction occurs through C–H bond activation or C=C double bond epoxidation. We have previously shown that C–H bond activation is preferred over C=C double bond epoxidation in the oxidation of cyclohexene by nonheme IS  $\text{Fe}^{\text{IV}}\text{O}$  and other  $\text{M}^{\text{IV}}\text{O}$  complexes (Scheme 1 B, pathway *a*), whereas the C=C double bond epoxidation is the preferred pathway in the oxidation of deuterated cyclohexene ( $[\text{D}_{10}]$ cyclohexene; Scheme 1 B, pathway *b*).<sup>[10]</sup> In the present study, we compared the chemoselectivity in the oxidation of cyclohexene and  $[\text{D}_{10}]$ cyclohexene by nonheme IS and HS  $\text{Fe}^{\text{IV}}\text{O}$  complexes **1** and **2** (Scheme 1 B). Upon addition of cyclohexene to a solution of **1**, the absorption band at  $\lambda = 770$  nm attributable to **1** disappeared with the first-order kinetic profile (Figure S5a). Pseudo-first-order rate constants, determined by the first-order fitting of the kinetic data for the decay of **1** (see Figure S5a, inset), increased linearly with the increase of the cyclohexene concentration (Figure 2, black line), giving a second-order rate constant of  $17(2) \text{ M}^{-1} \text{ s}^{-1}$  at  $-40^\circ\text{C}$ . When **1** was reacted with  $[\text{D}_{10}]$ cyclohexene, **1** decayed much more slowly, giving a second-order rate constant of  $2.1(2) \text{ M}^{-1} \text{ s}^{-1}$  at  $-40^\circ\text{C}$  (Figure 2, red line). Thus, the reaction of **1** with cyclohexene was 8.1(6) times faster than that of **1** with  $[\text{D}_{10}]$ cyclohexene.

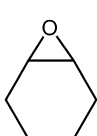
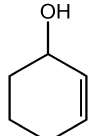
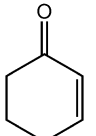
A similar reactivity pattern was detected in the oxidation of cyclohexene and  $[\text{D}_{10}]$ cyclohexene by a HS  $\text{Fe}^{\text{IV}}\text{O}$  complex **2**. Upon addition of cyclohexene and  $[\text{D}_{10}]$ cyclohexene to a solution of **2** at  $-40^\circ\text{C}$ , the absorption band at  $\lambda = 650$  nm corresponding to **2** disappeared (Figure S5b). The pseudo-first-order rate constants increased linearly with the increase of the substrate concentrations to give second-order rate constants of  $1.2(1) \times 10^2$  and  $5.1(4) \text{ M}^{-1} \text{ s}^{-1}$  in the reactions of cyclohexene and  $[\text{D}_{10}]$ cyclohexene, respectively (Figure 2, blue and green lines). Thus, **2** reacted with cyclohexene 24(2) times faster than with  $[\text{D}_{10}]$ cyclohexene.

We then analyzed products formed in the oxidation of cyclohexene and  $[\text{D}_{10}]$ cyclohexene by **1** and **2** under an Ar atmosphere (Table 1). The oxidation of cyclohexene by **1** and **2** afforded allylic oxidation products predominantly (namely cyclohexenol and cyclohexenone). In contrast, oxidation of



**Figure 2.** Plots of pseudo-first-order rate constants ( $k_{\text{obs}}$ ) against concentrations of cyclohexene (black line for **1** and blue line for **2**) and  $[\text{D}_{10}]$ cyclohexene (red line for **1** and green line for **2**). The plots are used to determine second-order rate constants ( $k_2$ ) in the oxidation of cyclohexene and  $[\text{D}_{10}]$ cyclohexene by **1** and **2** in  $\text{CH}_3\text{CN}$  at  $-40^\circ\text{C}$ .

**Table 1:** Products obtained in the oxidation of cyclohexene and  $[\text{D}_{10}]$ cyclohexene by **1** and **2**.<sup>[a]</sup>

	Substrate	Product Yield [%]		
				
<b>1</b>	cyclohexene	N.D.	27(3)	11(3)
	$[\text{D}_{10}]$ cyclohexene	34(3)	25(3)	4(2)
<b>2</b>	cyclohexene	N.D.	23(3)	14(3)
	$[\text{D}_{10}]$ cyclohexene	30(4)	17(4)	8(2)

[a] Reactions were run with intermediates **1** or **2** (1.0 mM) and substrates cyclohexene or  $[\text{D}_{10}]$ cyclohexene (100 mM) under an Ar atmosphere in  $\text{CH}_3\text{CN}$  at  $-40^\circ\text{C}$ . Values in parentheses indicate the estimated standard deviations. N.D. = not detected.

$[\text{D}_{10}]$ cyclohexene by **1** and **2** led primarily to the formation of the epoxide. These results imply that the cyclohexene oxidation by **1** and **2** occurs mainly through the C–H bond activation pathway (Scheme 1 B, pathway *a*), whereas the  $[\text{D}_{10}]$ cyclohexene oxidation by **1** and **2** preferentially occurs through C=C double bond epoxidation with concurrent C–H bond activation (Scheme 1 B, pathway *b*). We previously proposed that this change of mechanisms in the oxidation of cyclohexene and  $[\text{D}_{10}]$ cyclohexene by nonheme  $\text{M}^{\text{IV}}\text{O}$  complexes is due to the different C–H(D) bond strengths of the allylic C–H and C–D bonds in the substrates.<sup>[10b,11]</sup>

We also analyzed the iron products obtained in the oxidation of cyclohexene and  $[\text{D}_{10}]$ cyclohexene by **1** and **2**. First, in the oxidation of cyclohexene by **1** and **2**, EPR spectra of the reaction solutions exhibited signals at  $g = 7.4, 4.3$ , and  $2.00$  for **1** and  $g = 9.2, 4.3$ , and  $2.00$  for **2** (Figure S6, black lines), characteristic of high-spin  $\text{Fe}^{\text{III}}$  species ( $S = 5/2$ ). In CSI-MS experiments, we detected ion peaks at mass-to-charge ratios  $m/z = 671.1$  and  $261.1$  in the reaction of **1** and cyclohexene (Figure S7a). These ion peaks correspond to  $[\text{Fe}^{\text{III}}(\text{OH})(\text{Me}_3\text{NTB})(\text{CF}_3\text{SO}_3)]^+$  (calculated  $m/z = 671.1$ ) and  $[\text{Fe}^{\text{III}}(\text{OH})(\text{Me}_3\text{NTB})]^{2+}$  (calculated  $m/z = 261.1$ ), respec-

tively. In the case of **2**, we detected one ion peak at  $m/z = 662.1$  (Figure S7b), which corresponds to  $[\text{Fe}^{\text{III}}(\text{OH})(\text{TQA})(\text{CF}_3\text{SO}_3)]^+$  (calculated  $m/z = 662.1$ ). In the oxidation of  $[\text{D}_{10}]$ cyclohexene by **1** and **2**, intensities of the EPR signals corresponding to high-spin  $\text{Fe}^{\text{III}}$  species ( $S = 5/2$ ) were weaker than those obtained in the cyclohexene oxidation reactions (Figure S6, red lines). This observation implies that EPR-silent  $\text{Fe}^{\text{II}}$  species were also formed in the  $[\text{D}_{10}]$ cyclohexene reactions (see below). In the CSI-MS experiments, in addition to the ion peaks corresponding to  $\text{Fe}^{\text{III}}$  species, ion peaks corresponding to  $\text{Fe}^{\text{II}}$  species were also present (data not shown). Thus, based on the spectroscopic analyses of the reaction solutions, we conclude that  $\text{Fe}^{\text{III}}$  species, not  $\text{Fe}^{\text{II}}$  species, were formed as the products in the oxidation of cyclohexene by **1** and **2** (Scheme 1B, pathway *a*). In contrast, both  $\text{Fe}^{\text{III}}$  and  $\text{Fe}^{\text{II}}$  species were formed in the oxidation of  $[\text{D}_{10}]$ cyclohexene by **1** and **2** (Scheme 1B, pathway *b*). These results should also be considered in terms of the detection of  $\text{Fe}^{\text{III}}$  species as the product of C–H bond activation (see above) and  $\text{Fe}^{\text{II}}$  species as the product of C=C double bond epoxidation (see below for the epoxidation of styrene).

Finally, we considered the role of nonheme IS and HS  $\text{Fe}^{\text{IV}}\text{O}$  complexes **1** and **2** in the epoxidation of styrene and deuterated styrene  $[\text{D}_8]$ styrene. In these reactions, the reactivity of **1** was greater than that of **2**, in contrast to that detected for the C–H bond activation of alkanes and the oxidation of cyclohexene (see above). We also found that for complexes **1** and **2** the rates of the oxidation of styrene and  $[\text{D}_8]$ styrene were the same (kinetic isotope effect  $\text{KIE} = 1$ ; see Figure S8). We also observed this effect in the reaction of nonheme  $\text{Fe}^{\text{IV}}\text{O}$  and  $\text{Ru}^{\text{IV}}\text{O}$  complexes.<sup>[10b,11]</sup> Product analysis of the reaction solutions revealed that styrene oxide was the predominant product (Table S1). The source of the oxygen atom in the styrene oxide was found to be the  $\text{Fe}^{\text{IV}}\text{O}$  complexes, not  $^{18}\text{O}_2$ , when the styrene epoxidation by **1** and **2** was carried out under an  $^{18}\text{O}_2$  atmosphere (Figure S9). In addition, the decayed iron products of **1** and **2** were  $\text{Fe}^{\text{II}}$  species when the reaction solutions were analyzed by EPR spectroscopy; EPR spectra of the reaction solutions were silent (see Figure S6, blue lines). These results demonstrate that **1** and **2** oxidized styrene to styrene oxide through the C=C double bond epoxidation mechanism (Scheme 1C).

The styrene epoxidation by **1** and **2** was also carried out with *para*-X-substituted styrene derivatives (4-X-styrenes; X = MeO, Me, H, Cl, and  $\text{NO}_2$ ) and 3-Cl-styrene. In these reactions, we obtained a good linear correlation with similar slopes of  $-1.6$  and  $-1.8$  for **1** and **2**, respectively, when the second-order rate constants were plotted against oxidation potentials ( $E_{\text{ox}}$ ) of styrene derivatives (Figure 3). These results indicate that **1** and **2** oxidize the styrene derivatives through an oxygen atom transfer mechanism<sup>[16]</sup> with similar electrophilic character. We therefore conclude that the oxidation of styrene derivatives by **1** and **2** occurs through the C=C epoxidation pathway and that the electrophilic characters of **1** and **2** are similar in the olefin epoxidation reactions.

In conclusion, we have compared the reactivities of synthetic nonheme IS and HS  $\text{Fe}^{\text{IV}}\text{O}$  complexes in three different oxidation reactions. Unexpectedly, the reaction

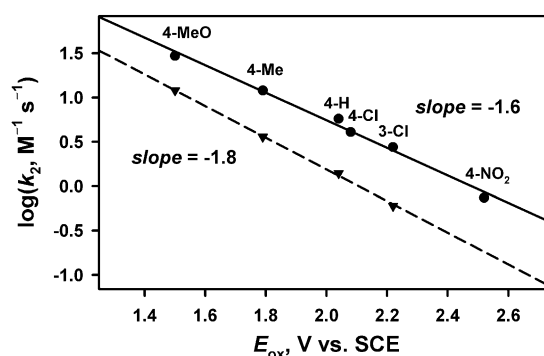


**Figure 3.** Plots of  $\log k_2$  against  $E_{\text{ox}}$  values for 4-X-styrenes (X = MeO, Me, H, Cl, and  $\text{NO}_2$ ) and 3-Cl-styrene in the oxidation reactions of styrene derivatives by **1** (solid line) and **2** (dotted line) in  $\text{CH}_3\text{CN}$  at  $-40^\circ\text{C}$ . SCE = standard calomel electrode.

mechanisms and reactivity patterns of the nonheme IS and HS  $\text{Fe}^{\text{IV}}\text{O}$  complexes are not different in the C–H bond activation of alkanes, the oxidation of cyclohexene, and the epoxidation of styrene derivatives. However, the question still remains as to why mononuclear nonheme iron enzymes use HS  $\text{Fe}^{\text{IV}}\text{O}$  intermediates in their enzymatic oxidation reactions. This is a key issue that should be addressed in future biological and biomimetic studies of nonheme iron enzymes.

### Acknowledgements

The authors acknowledge financial support from the NRF of Korea through the CRI (NRF-2012R1A3A2048842 to W.N.), the GRL (NRF-2010-00353 to W.N.), and the MSIP (NRF-2013R1A1A2062737 to K.-B.C.).

**Keywords:** bioinorganic chemistry · C–H activation · iron · metalloenzymes · reaction mechanisms

- [1] a) C. Krebs, D. G. Fujimori, C. T. Walsh, J. M. Bollinger, Jr., *Acc. Chem. Res.* **2007**, *40*, 484–492; b) S. D. Wong, M. Srncic, M. L. Matthews, L. V. Liu, Y. Kwak, K. Park, C. B. Bell III, E. E. Alp, J. Zhao, Y. Yoda, S. Kitao, M. Seto, C. Krebs, J. M. Bollinger, Jr., E. I. Solomon, *Nature* **2013**, *499*, 320–324.
- [2] a) J. C. Price, E. W. Barr, B. Tirupati, J. M. Bollinger, Jr., C. Krebs, *Biochemistry* **2003**, *42*, 7497–7508; b) J.-U. Rohde, J.-H. In, M. H. Lim, W. W. Brennessel, M. R. Bukowski, A. Stubna, E. Münck, W. Nam, L. Que, Jr., *Science* **2003**, *299*, 1037–1039.
- [3] a) W. Nam, *Acc. Chem. Res.* **2007**, *40*, 522–531; b) J. Hohenberger, K. Ray, K. Meyer, *Nat. Commun.* **2012**, *3*, 720; c) K. Ray, F. F. Pfaff, B. Wang, W. Nam, *J. Am. Chem. Soc.* **2014**, *136*, 13942–13958; d) W. Nam, Y.-M. Lee, S. Fukuzumi, *Acc. Chem. Res.* **2014**, *47*, 1146–1154; e) S. A. Cook, A. S. Borovik, *Acc. Chem. Res.* **2015**, *48*, 2407–2414; f) M. Puri, L. Que, Jr., *Acc. Chem. Res.* **2015**, *48*, 2443–2452.
- [4] a) O. Pestovsky, S. Stoian, E. L. Bominaar, X. Shan, E. Münck, L. Que, Jr., A. Bakac, *Angew. Chem. Int. Ed.* **2005**, *44*, 6871–6874; *Angew. Chem.* **2005**, *117*, 7031–7034; b) J. England, M. Martinho, E. R. Farquhar, J. R. Frisch, E. L. Bominaar, E. Münck, L. Que, Jr., *Angew. Chem. Int. Ed.* **2009**, *48*, 3622–3626; *Angew. Chem.* **2009**, *121*, 3676–3680; c) J. England, Y.

- Guo, E. R. Farquhar, V. G. Young, Jr., E. Münck, L. Que, Jr., *J. Am. Chem. Soc.* **2010**, *132*, 8635–8644; d) D. C. Lacy, R. Gupta, K. L. Stone, J. Greaves, J. W. Ziller, M. P. Hendrich, A. S. Borovik, *J. Am. Chem. Soc.* **2010**, *132*, 12188–12190; e) J. England, Y. Guo, K. M. V. Heuvelen, M. A. Cranswick, G. T. Rohde, E. L. Bominaar, E. Münck, L. Que, Jr., *J. Am. Chem. Soc.* **2011**, *133*, 11880–11883; f) J. P. Bigi, W. H. Harman, B. Lassalle-Kaiser, D. M. Robles, T. A. Stich, J. Yano, R. D. Britt, C. J. Chang, *J. Am. Chem. Soc.* **2012**, *134*, 1536–1542; g) D. J. Xiao, E. D. Bloch, J. A. Mason, W. L. Queen, M. R. Hudson, N. Planas, J. Borycz, A. L. Dzubak, P. Verma, K. Lee, F. Bonino, V. Crocellà, J. Yano, S. Bordiga, D. G. Truhlar, L. Gagliardi, C. M. Brown, J. R. Long, *Nat. Chem.* **2014**, *6*, 590–595.
- [5] A. N. Biswas, M. Puri, K. K. Meier, W. N. Oloo, G. T. Rohde, E. L. Bominaar, E. Münck, L. Que, Jr., *J. Am. Chem. Soc.* **2015**, *137*, 2428–2431.
- [6] a) H. Chen, W. Lai, S. Shaik, *J. Phys. Chem. Lett.* **2010**, *1*, 1533–1540; b) S. Shaik, H. Chen, D. Janardanan, *Nat. Chem.* **2011**, *3*, 19–27.
- [7] a) M. Puri, A. N. Biswas, R. Fan, Y. Cuo, L. Que, Jr., *J. Am. Chem. Soc.* **2016**, *138*, 2484–2487; b) E. Andris, J. Jašík, L. Gómez, M. Costas, J. Roithová, *Angew. Chem. Int. Ed.* **2016**, *55*, 3637–3641; *Angew. Chem.* **2016**, *128*, 3701–3705.
- [8] M. S. Seo, N. H. Kim, K.-B. Cho, J. E. So, S. K. Park, M. Clémancey, R. Garcia-Serres, J.-M. Latour, S. Shaik, W. Nam, *Chem. Sci.* **2011**, *2*, 1039–1045.
- [9] K.-B. Cho, X. Wu, Y.-M. Lee, Y. H. Kwon, S. Shaik, W. Nam, *J. Am. Chem. Soc.* **2012**, *134*, 20222–20225.
- [10] a) K.-B. Cho, H. Hirao, S. Shaik, W. Nam, *Chem. Soc. Rev.* **2016**, *45*, 1197–1210; b) S. N. Dhuri, K.-B. Cho, Y.-M. Lee, S. Y. Shin, J. H. Kim, D. Mandal, S. Shaik, W. Nam, *J. Am. Chem. Soc.* **2015**, *137*, 8623–8632; c) K.-B. Cho, H. Kang, J. Woo, Y. J. Park, M. S. Seo, J. Cho, W. Nam, *Inorg. Chem.* **2014**, *53*, 645–652; d) K.-B. Cho, S. Shaik, W. Nam, *J. Phys. Chem. Lett.* **2012**, *3*, 2851–2856; e) X. Wu, M. S. Seo, K. M. Davis, Y.-M. Lee, J. Chen, K.-B. Cho, Y. N. Pushkar, W. Nam, *J. Am. Chem. Soc.* **2011**, *133*, 20088–20091.
- [11] Y. H. Kwon, B. K. Mai, Y.-M. Lee, S. N. Dhuri, D. Mandal, K.-B. Cho, Y. Kim, S. Shaik, W. Nam, *J. Phys. Chem. Lett.* **2015**, *6*, 1472–1476.
- [12] S. Rana, A. Dey, D. Maiti, *Chem. Commun.* **2015**, *51*, 14469–14472.
- [13] a) J. T. Groves, *J. Chem. Educ.* **1985**, *62*, 928–931; b) A. S. Borovik, *Chem. Soc. Rev.* **2011**, *40*, 1870–1874; c) S. A. Cook, E. A. Hill, A. S. Borovik, *Biochemistry* **2015**, *54*, 4167–4180.
- [14] a) S. Martinez, R. P. Hausinger, *J. Biol. Chem.* **2015**, *290*, 20702–20711; b) M. A. Bigi, S. A. Reed, M. C. White, *Nat. Chem.* **2011**, *3*, 216–222; c) L. Ji, A. S. Faponle, M. G. Quesne, M. A. Sainna, J. Zhang, A. Franke, D. Kumar, R. van Eldik, W. Liu, S. P. de Visser, *Chem. Eur. J.* **2015**, *21*, 9083–9092; d) W. Lai, H. Chen, S. Cohen, S. Shaik, *J. Phys. Chem. Lett.* **2011**, *2*, 2229–2235.
- [15] a) S. Kundu, J. V. K. Thompson, L. Q. Shen, M. R. Mills, E. L. Bominaar, A. D. Ryabov, T. J. Collins, *Chem. Eur. J.* **2015**, *21*, 1803–1810; b) E. Kwon, K.-B. Cho, S. Hong, W. Nam, *Chem. Commun.* **2014**, *50*, 5572–5575.
- [16] a) J. Park, Y. Morimoto, Y.-M. Lee, W. Nam, S. Fukuzumi, *Inorg. Chem.* **2014**, *53*, 3618–3628; b) J. Chen, H. Yoon, Y.-M. Lee, M. S. Seo, R. Sarangi, S. Fukuzumi, W. Nam, *Chem. Sci.* **2015**, *6*, 3624–3632.

Received: April 25, 2016

Published online: ■ ■ ■ ■ ■, ■ ■ ■ ■ ■

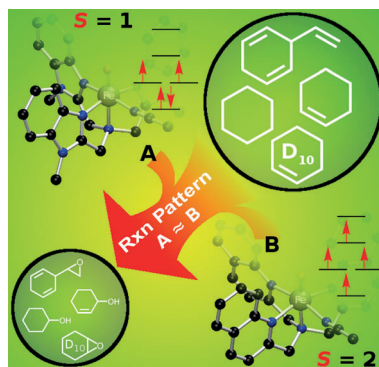
## Communications



## Bioinorganic Chemistry

S. H. Bae, M. S. Seo, Y.-M. Lee, K.-B. Cho,  
W.-S. Kim, W. Nam\* ——— ■■■■—■■■■

Mononuclear Nonheme High-Spin ( $S=2$ ) versus Intermediate-Spin ( $S=1$ )  
Iron(IV)–Oxo Complexes in Oxidation  
Reactions



**Biomimetics:** The reactivities of synthetic mononuclear nonheme high-spin ( $S=2$ ) and intermediate-spin ( $S=1$ ) iron(IV)–oxo complexes were studied. The complexes were found to exhibit similar reaction mechanisms and reactivity patterns in a C–H bond activation reaction of alkanes, the oxidation of cyclohexene, and the epoxidation of styrene.